Supporting information for:

Enormous Lattice Distortion Through Isomorphous Phase Transition in Organic-Inorganic Hybrid Based on Haloantimonate(III)

Martyna Wojciechowska[a], Przemysław Szklarz[a], Agata Białońska[a], Jan Baran[b], Rafał Janickia, Wojciech Medycki[c], Piotr Durlak[a], Anna Piecha-Bisiorek*[a] and Ryszard Jakubas[a]

[a]*Faculty of Chemistry, University of Wrocław, Joliot-Curie 14, 50-383 Wrocław, Poland*
[b]*Institute of Low Temperature and Structure Research, Polish Academy of Science, Okólna 2, 50-950 Wrocław 2, PO Box 937, Poland*
[c]*Institute of Molecular Physics, PAS, M. Smoluchowskiego 17, 60-179 Poznań, Poland*

Contents:

.

Crystal data				
Empirical formula	$C_8H_{20}NSbBr_4$		C_8H_{20} $NSbCl_4$	
Formula weight (g mol^{-1})	571.64		393.80	
Crystal system	Monoclinic		Monoclinic	
Space group	$P2_1/c$		$P2_1/c$	
Unit cell dimensions				
a (Å)	5.964(2)	6.046(2)	5.790(2)	5.750(2)
b (Å)	20.098(8)	18.186(3)	19.485(3)	19.314(3)
c (Å)	14.385(8)	14.839(3)	14.275(3)	14.248(3)
β (°)	99.25(5)	96.32(2)	101.28(3)	101.99(2)
V (Å^3)	1701.8(13)	1621.7(7)	1579.4(7)	1547.8(7)
Z	4		4	
$D_{calc.}$ (g cm^{-3})	2.231	2.341	2.395	2.444
μ [mm^{-1}]	10.987	11.530	2.395	2.444
Crystal size	0.50x0.24x0.18		0.35x0.13x0.10	0.21x0.14x0.09
Data collection and Refinement				
Temperature	250(2) K	100(2) K	250(2) K	100(2)
Final R indices [I>2sigma(I)]	R1 = 0.046, wR2 = 0.113	R1 = 0.032, wR2 = 0.072	R1 = 0.034, wR2 = 0.059	R1 = 0.029, wR2 = 0.078

Table S1 Experimental data for $[(i\text{-}C_4H_9)_2NH_2]_2Sb_2Br_8$ and $[(i\text{-}C_4H_9)_2NH_2]_2Sb_2Cl_8$

Diffractometer: Xcalibur, Sapphire2, large Be window; Monochromator: Graphite; Radiation type, wavelength λ (Å): MoKα, 0.71073; Absorption correction: Analytical; Refinement method: Full-matrix least-squares on F^2

X-ray diffraction studies The crystallographic measurements were performed on a Kuma KM4CCD four-circle diffractometer with the graphite monochromatized MoKα radiation. The data sets were collected at 100(2) K and 250(2) K using the Oxford Cryosystems cooler and analytically corrected for absorption with the use of the CrysAlis RED program[1] and the KM4CCD software, using a multifaceted crystal model based on the research of Clark and Reid.[2] The crystal structures were solved by direct methods with the SHELXS-97 program and refined by a full-matrix least-squares method on all F^2 data using the SHELXL-97 program.[3] All non-H atoms were refined with anisotropic temperature factors. However, ISOR, SIMU and SADI restraints were applied for the disordered cation at 250 K. Occupancy factors of components of the disordered cation were determined assuming that the sum of all components is equal to 1. The H atoms were located from the molecular geometry and their isotropic temperature factors U_{iso} were assumed as 1.2 or 1.5 times U_{eq} of their parent atoms. The crystal data together with experimental and refinement details are given in Table 3. Crystallographic data for the structure reported in this paper (excluding structure factors) have been deposited with the Cambridge Crystallographic Data Centre,

1 CrysAlis RED, ver. 1.171, Oxford Diffraction Poland (1995–2003).
2 R. C. Clark, J. S. Reid, *Acta Cryst*., 1995, **A51**, 887.
3 G. M. Sheldrick, *Acta Cryst*., 2008, **A64**, 112.

Table S2. Selected bond lengths (Å) and angels (°) for $[(i\text{-}C_4H_9)_2NH_2]_2Sb_2Cl_8$

at 250 K		**at 100 K**	
Sb-Cl(1)	2.3697(13)	Sb-Cl(1)	2.3777(9)
Sb-Cl(2)	3.0442(14)	Sb-Cl(2)	3.0482(6)
Sb-Cl(2)^{i}	3.0143(13)	Sb-Cl(2)^{ii}	2.9839(8)
Sb-Cl(3)	2.3941(13)	Sb-Cl(3)	2.3983(6)
Sb-Cl(4)	2.3975(13)	Sb-Cl(4)	2.4069(7)
Sb-Cl(1)^{ii}	3.4886(16)	Sb-Cl(1)^{ii}	3.4523(12)
Cl(1)-Sb-Cl(3)	92.02(5)	Cl(1)-Sb-Cl(3)	91.661(16)
Cl(1)-Sb-Cl(4)	94.07(6)	Cl(1)-Sb-Cl(4)	93.85(3)
Cl(3)-Sb-Cl(4)	92.26(5)	Cl(3)-Sb-Cl(4)	92.188(16)
Cl(1)-Sb-Cl(2)	84.17(4)	Cl(1)-Sb-Cl(2)	83.559(14)
Cl(3)-Sb-Cl(2)	176.15(4)	Cl(3)-Sb-Cl(2)	175.202(15)
Cl(4)-Sb-Cl(2)	88.62(4)	Cl(4)-Sb-Cl(2)	88.563(15)

Symmetry codes $^{(i)}$: 1-x; 1-y; -z; $^{(ii)}$ 1+x, y, z

Table S3. Hydrogen bonds for $[(i\text{-}C_4H_9)_2NH_2]_2Sb_2Cl_8$ [Å and °] (250 K/100 K).

D-H...A	d(D-H)	d(H...A)	d(D...A)	<(DHA)>
N1-H12...Cl(2)	0.91/0.91	2.44/2.40	3.276(4)/3.2390(17)	153/154
N1-H11...Cl(2)[i]	0.91/0.91	2.52/2.48	3.224(4)/3.1962(18)	135/135

[i] x-1,y,z

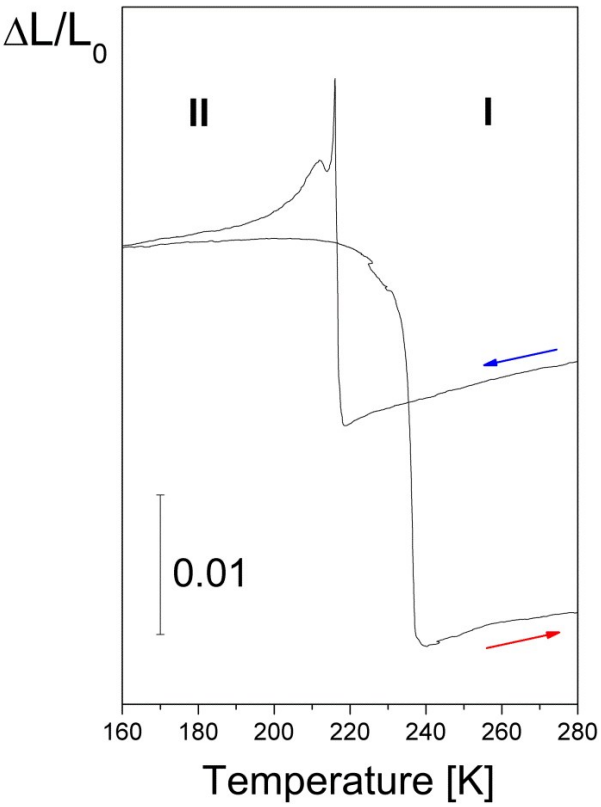

Figure S1. The linear thermal expansion for the polycrystalline sample of $[(i\text{-}C_4H_9)_2NH_2]_2Sb_2Br_8$ upon cooling and heating.

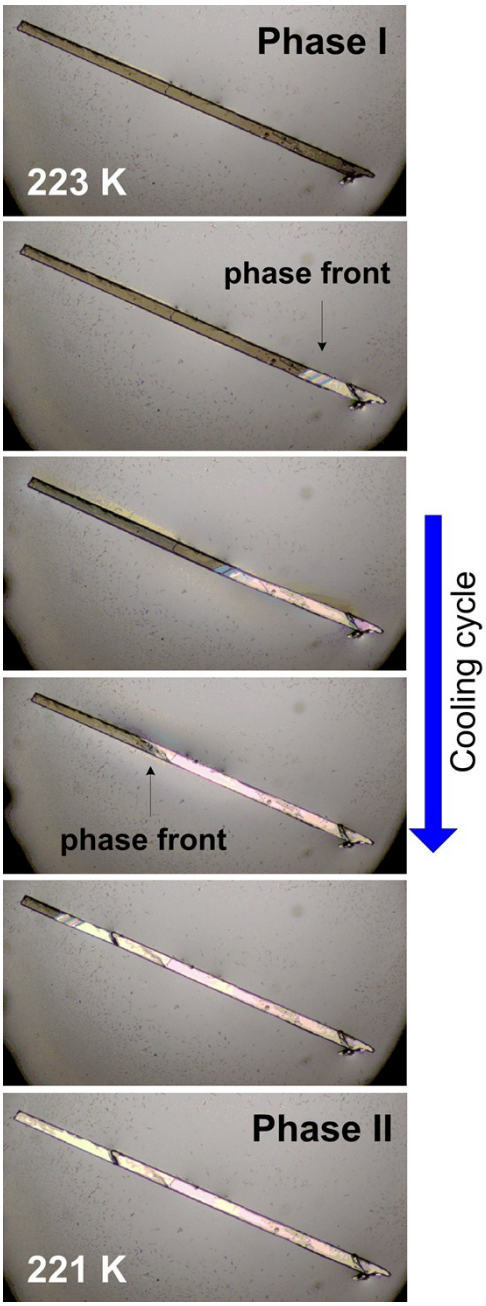

Figure S2. Polarized light microscopy photographs of $[(i\text{-}C_4H_9)_2NH_2]_2Sb_2Br_8$ in the ac plane taken at several temperatures (rate: 0.1 K/min) in the close vicinity of T_c (see also Film F1)

This effect is seen well and is reversible only at a very slow scans rate. A faster change of temperature makes the crystal bounce off the surface or burst. Given this phenomenon, it is clear why we were not able to obtain high quality results of the complex dielectric permittivity on the crystal sample.

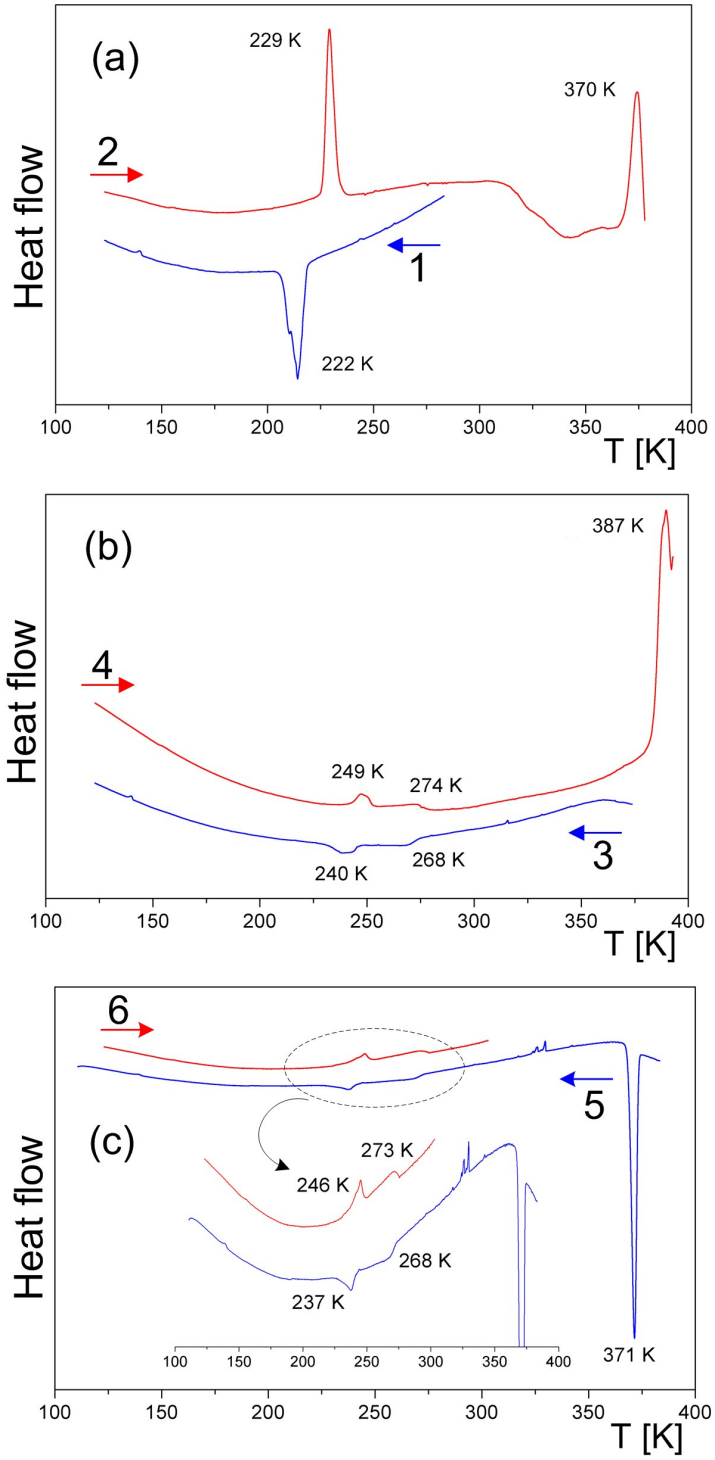

Figure S3. DSC traces upon cooling and heating (5 K/min) for $[(i\text{-}C_4H_9)_2NH_2]_2Sb_2Br_8$ (m= 10.622 mg)

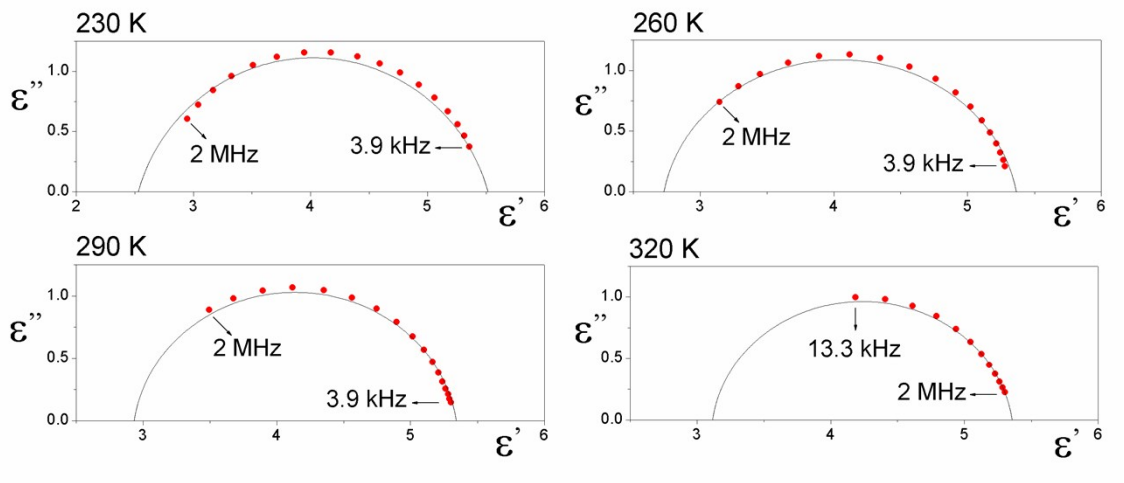

Figure S4. Cole–Cole plots of ε'' *vs*. ε' at four selected temperatures showing a relaxation nature of the dielectric dispersion in $[(i\text{-}C_4H_9)_2NH_2]_2Sb_2Br_8$.

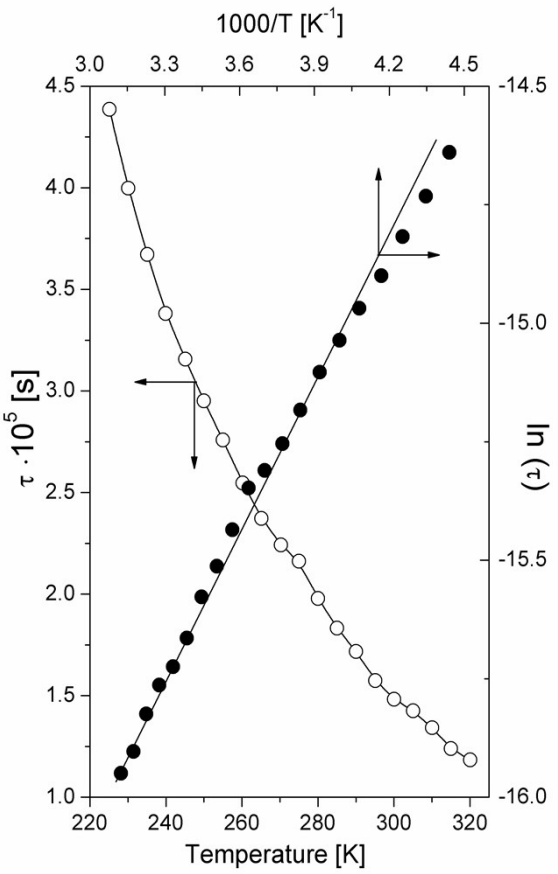

Figure S5. Cole Temperature dependence of τ *vs*. temperature and ln τ *vs*. reciprocal temperature obtained from the Cole–Cole formula over the phase I of $[(i\text{-}C_4H_9)_2NH_2]_2Sb_2Br_8$.

The total T_1 relaxation time can be expressed using the Woessner formula for complex compounds:[35]

$$\frac{1}{T_1} = \frac{6}{20}\frac{1}{T_1^{CH_3^{I}}(\tau_{cI})} + \frac{6}{20}\frac{1}{T_1^{CH_3^{II}}(\tau_{cII})} + \frac{8}{20}\frac{1}{T_1^{H_i}},$$

where: the relaxation time of the CH_3 group is described by the following formula:

$$\frac{1}{T_1^{CH_3}} = \frac{9}{20}\frac{\gamma^4 \hbar^2}{r_{CH_3}^6}\left(\frac{\tau_c}{1+\omega_0^2\tau_c^2} + \frac{4\tau_c}{1+4\omega_0^2\tau_c^2}\right)$$

where: r_{CH3} is the proton-proton distance in the CH_3 group, τ_{cI} and τ_{cII} are the correlation times of the two types of methyl groups, the number 6 in numerator denotes number of protons of two CH_3 groups of the side chain of the cation, the number 20 in the denominator means the number of protons in one cation. It seems that the rest of eight skeletal protons in each cation (besides 12 protons of four methyl groups) in compliance with the assumed spin diffusion are relaxing enough slowly and the third component relaxation time in equation (6) should be negligible. The temperature dependence of correlation times in the temperature range of the fit is described by the Arrhenius law $\tau_{ci}=\tau_{oi}\exp(E_a/RT)$. The obtained parameters of the fit given in Table S4 are typical of the C_3-type relaxations of CH_3 groups.[36-45] When, in turn, will draw the above curve fitting using a frequency measurement 15 MHz we find that the line is passing nearly exactly over the measured points with slight deviations which we attribute to the presence of the interacting quadrupole nuclei, mainly halogens ones. In turn, the measured points over the phase I reveal only part of one minimum of T_1 relaxation time.

Table S4. Motional parameters obtained from fitting of the theoretical line (eq. 5) to date points for $[(i\text{-}C_4H_9)_2NH_2]_2Sb_2Br_8$

T_{min} [K]	E_a [kcal/mol]	τ_{c1} [s]	C [10^9 s^{-2}]
126	2.28	7.83 10^{-13}	2.18
144	2.5	1.56 10^{-12}	1.96
295	2.87	2.95 10^{-11}	1.99

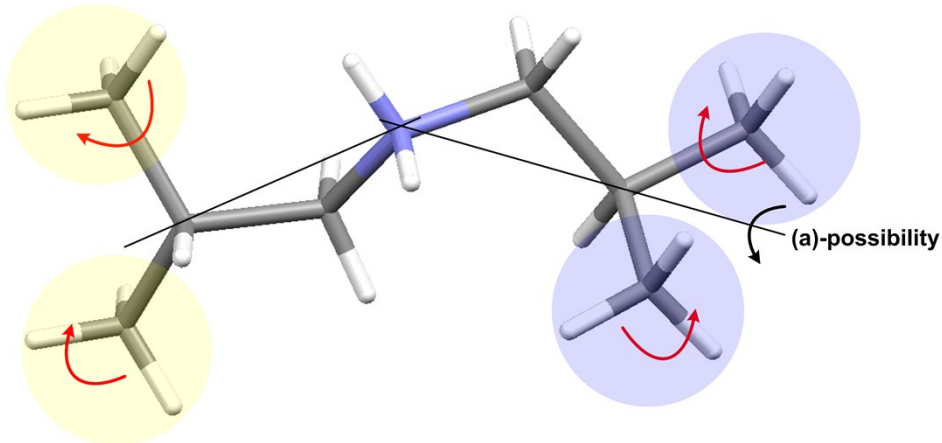

Figure S6 Possible type of motions within the diisobutyloammonium cation. Yellow and violet circles denote two unequivalent pairs of methyl groups.

Considering coupling between the normal modes of the symmetry equivalent ions (Davydov type splitting), each A type normal mode splits into four $A_g+B_g+A_u+B_u$ unit cell modes, whereas the A_g type normal mode splits into two A_g + B_g unit cell modes, and the A_u type normal modes split into two A_u + B_u unit cell modes. The collection of the fundamental modes (k =0; unit cell modes) for the low temperature phase are given in the Table S5.

Table S5. Fundamental modes analysis for the low temperature phase of the title crystal*

UCG	Lattice modes			Internal modes		Selection rules	
C_{2h}	Acoustic	Anion+Cations		$[Sb_2Br_8^{2-}]$	$[(i\text{-}C_4H_9)_2NH_2^{(+1)}]$	IR	Raman
		L	T				
A_g		6	3	12	81	i	xx,yy,zz, xz
B_g		6	3	12	81	i	xy, zy
A_u	1	3	5	12	81	Y	i
B_u	2	3	4	12	81	X, Z	i

*Abbreviations: UCG – unit cell group (i.e. factor group); Acoustic – acoustic modes; Anion - $Sb_2Br_8^{(2-)}$; Cation - $[(i\text{-}C_4H_9)_2NH_2^{(+1)}]$; L- librational modes; T- translational modes; IR – infrared spectroscopy; Raman – Raman spectroscopy; i – inactive

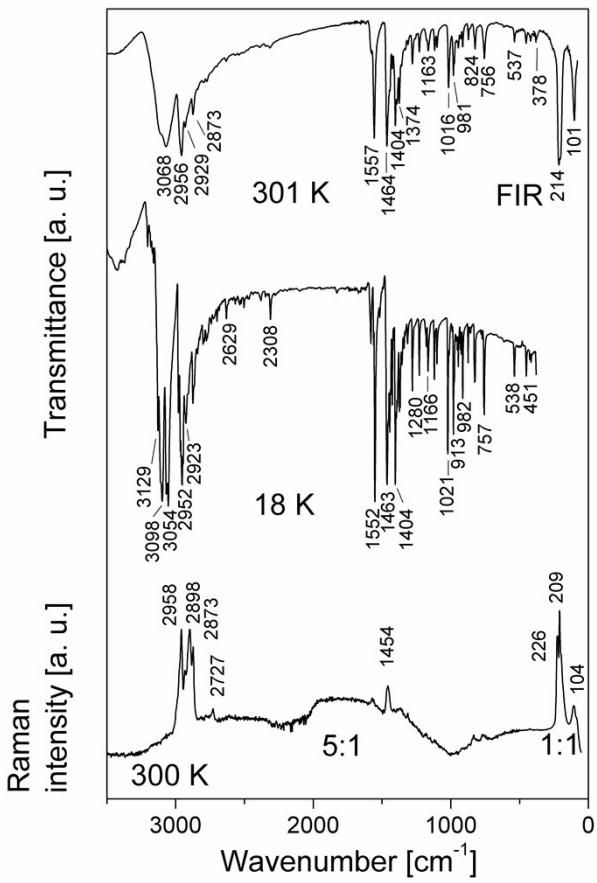

Figure S7. The infrared spectra of the powdered $[(i\text{-}C_4H_9)_2NH_2]_2Sb_2Br_8$ sample in KBr pellet (18 K and 301 K), FIR and the Raman spectra at 300 K.

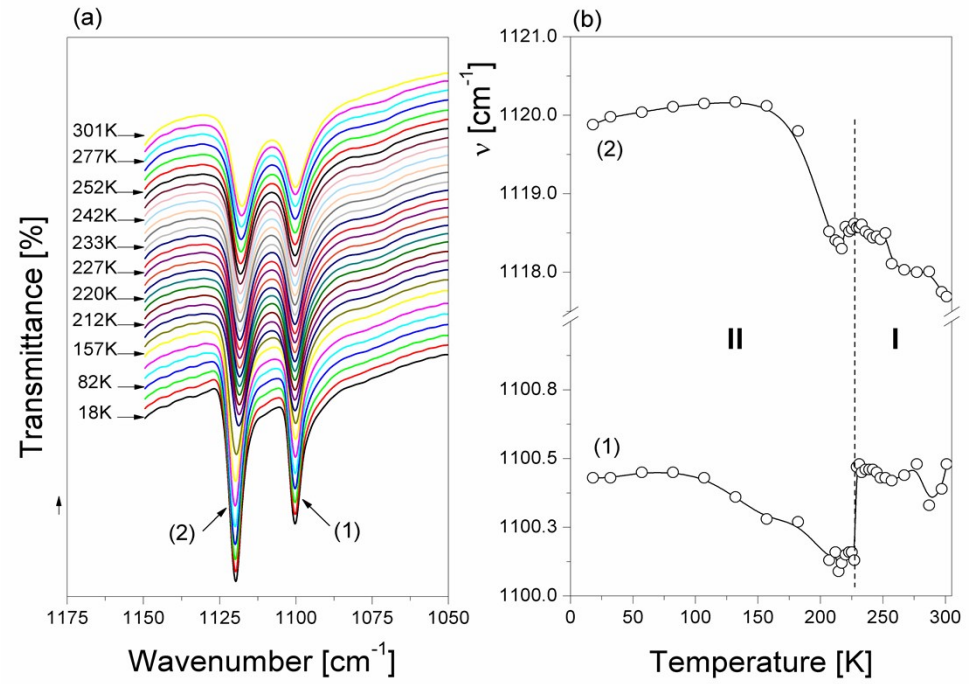

Figure S8. (a) Temperature evolution of the IR spectrum between 1050 and 1150 cm^{-1} (the ρCH_3); (b) the dependencies of the wavenumbers of the selected modes on the temperature change for the $[(i\text{-}C_4H_9)_2NH_2]_2Sb_2Br_8$.

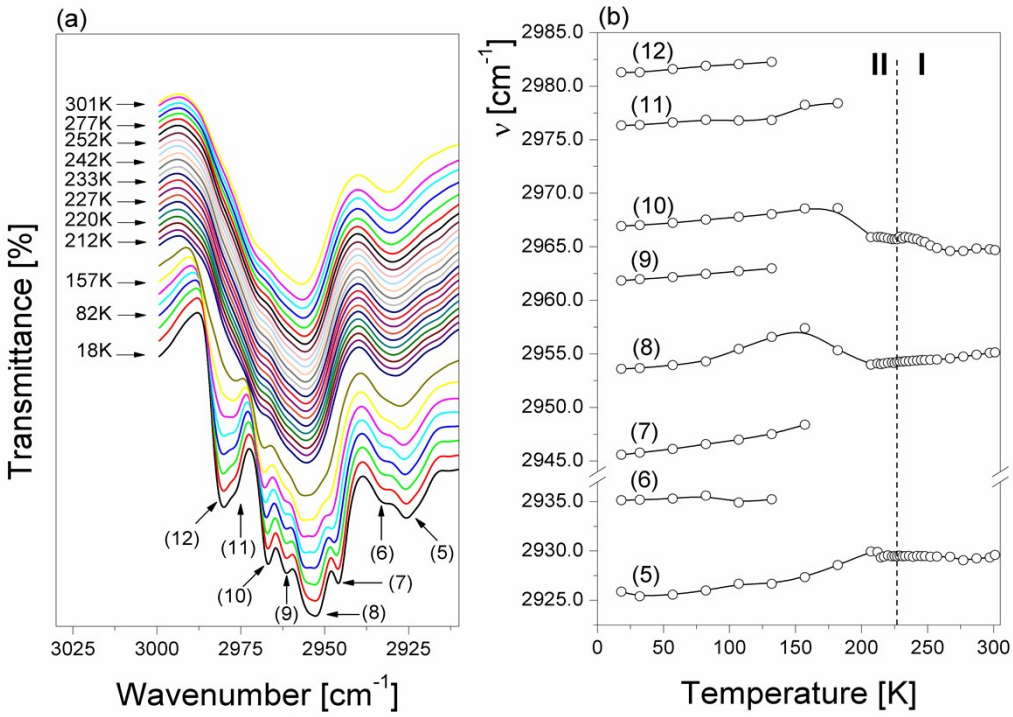

Figure S9. (a) Temperature evolution of the IR spectrum in the $\nu_a(CH_3)$ vibration region (2910–3000 cm^{-1}) and (b) the dependencies of the wavenumbers of these modes on the temperature change between 18 and 301 K for the $[(i\text{-}C_4H_9)_2NH_2]_2Sb_2Br_8$ crystal.

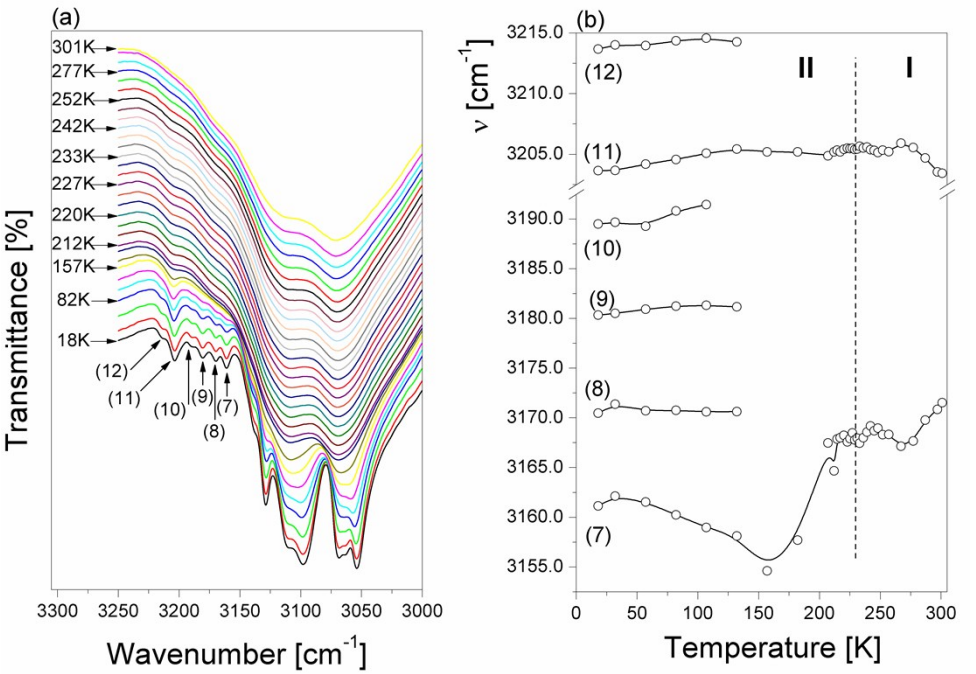

Figure S10. (a) Temperature evolution of the IR spectrum between 3250 and 3000 cm^{-1} ($\nu_a NH_2^+$ and $\nu_s NH_2^+$) (b) the dependencies of the wavenumbers the selected modes on the temperature change for the $[(i\text{-}C_4H_9)_2NH_2]_2Sb_2Br_8$.

Table S6. Wavenumbers (cm^{-1}) and relative intensities of the bands observed in the Infrared and Raman spectra of $[(i\text{-}C_4H_9)_2NH_2]_2Sb_2Br_8$ (IR at 18 and 301 K in KBr, Raman at 300 K).

Calculations IR/Raman	IR in KBr pellet		FT-Raman	TENTATIVE ASSIGNMENT
	T = 18 K	T = 301 K	T = 300 K	
	3214 vw			
	3204 vw	3204 vw sh		
	3190 vw sh			
	3180 svw			
	3170 vw			
	3161 vw	3171 msh		
	3138msh			
	3129 vs			
3365 vs	3111 vs	3114 m		$\nu_a(NH_2^+)$
	3098 vs			$\nu_a(NH_2^+)$
3329 vs	3069 vs	3069 vs		$\nu_a(NH_2^+)$ or $\nu_s(NH_2^+)$
	3064 vs			$\nu_a(NH_2^+)$ or $\nu_s(NH_2^+)$
	3054 vs			$\nu_a(NH_2^+)$ or $\nu_s(NH_2^+)$
3109 vs	2981 vs		2989 vwsh	$\nu_a(CH_3)$
	2976 vs		2975 vwsh	

3024 vs/3023 vs	2967 vs	2965 vssh		$\nu_a(CH_3)$
	2962 vs			$\nu_a(CH_3)$
3019 vs/3016 vs	2954 vssh	2957 vs	2959 w	$\nu_a(CH_3)$
	2952 vs			
3002 vs	2946 vs			$\nu_a CH_2$
	2935 ssh		2931vw	
	2926 s	2930 m		$V_a CH_2$
	2910 ssh	2912 msh	2911 vwsh	
	2889 msh	2894 msh	2898 w	$\nu(CH)$
	2875 s	2874 vs	2874 w	$\nu_s(CH_3)$ or $\nu(CH)$
	2863 s			$\nu_s(CH_2)$
	2853vssh			
	2841vw	2841w		$\nu_s CH_2$
	2833vwsh			
	2825vw			
	2811vwsh			O
	2801vw	2797w		V
	2791vw			E
	2797vw			R
	2776vw	2774w		T
	2769vw			O
	2763vw			N
	2748vw			E
	2741vw			S
	2724vw		2728 vw	
	2720vwsh			
	2715vwsh			O
	2700 w	2703vw		V
	2683vw			E
	2673vwsh			R
	2670vw			T
	2654vw			O
	2631w	2632w		N
	2620vw			E
	2607vw			S
	2598vw			
	2589vwsh			O
	2586vw			V
	2567vw	2569vw		E
	2558vw			R
	2543vwsh			T
	2540vw	2543vw		O
	2533vw			N
	2524vw			E
	2513vw			S
	2503vw	2506vw		

	2496vwsh			O
	2487vw			V
	2475vw	2474vw		E
	2467vw			R
	2459vwsh			T
	2442vwsh			O
	2436vw	2437vw		N
	2428vwsh			E
	2419vwsh			S
	2413vw			
	2399vwsh			O
	2391vwsh			V
	2380vw	2387w		E
	2347vw	2343wsh		R
	2337vw			T
	2329vw			O
	2311w	2314w		N
	2290vw			E
	2277vw			S
	2272vwsh			
	2263vwsh			O
	2254vw			V
	2277vwsh			E
	2220vw			R
	2199vw			T
	2193vw			O
	2183vw			N
	2164vw			E
	2143 vw			S
	2099 vw			
	2091 vwsh			
	1828 vw			
	1589 vwsh	1590vwsh		
	1583 wsh			$\delta(NH_2^+)$
	1582 w	1580wsh		$\delta(NH_2^+)$
	1573 wsh	1577w	1571vw	$\delta(NH_2^+)$
1639 m	1562 m			$\delta(NH_2^+)$
1638 vs	1552 vs	1557 vs		$\delta(NH_2^+)$
		1536wsh		$\delta(NH_2^+)$
	1467 vs	1464 vs		$\delta(CH_2)$
1547 vs	1463 vs			$\delta_a(CH_3)$ or $\delta(CH_2)$
1544 s	1456 s		1458 w	$\delta_a(CH_3)$ or $\delta(CH_2)$
1531 ssh	1452 ssh	1454msh		$\delta_a(CH_3)$
	1446 ssh	1449 msh		
	1443 s	1443 m		
	1438 s			
1522 s	1425 s	1426 w		δCH_2

	1414 w			
	1404 vs	1404 vs		
	1396 s			
	1389 m	1391 s		$\delta_s(CH_3)$ or $\delta(CH)$
	1375 s	1376 s		$\delta_s(CH_3)$
	1369 s	1372 ssh	1368 vwb	$\delta_s(CH_3)$
	1356 m	1359 m		$\delta(CH)$ or τCH_2
	1352 wsh	1351 msh		$\delta(CH)$ or τCH_2
1503 w	1340 w	1338wsh		ωCH_2
	1325vwsh			
1499 w	1332 w	1329 w		ωCH_2
1497 m	1315 m	1313 w		ωCH_2
	1313 msh	1308 w	1313 vw	ωCH_2
1392 m	1280 m	1280 m		ρCH_3
	1275 msh			
		1259wsh		
		1245vwsh		
1471 m	1230 m	1230 w		$\tau(CH_2)$ or $\tau(NH2^+\}$
	1184 wsh			
1422 w	1178 w	1176 w		$\nu_a(CH_3)_2C$
	1166m	1165 w		$\rho(CH_3)$
1209 wsh	1155 wsh			$\nu_a(CCC)$ or $\rho(CH_3)$
	1120 m	1118 w		$\rho(CH_3)$
	1100 m	1100 w		$\rho(CH_3)$
1129 s	1021 s	1016 s		$\nu_a CNC$
	1012 w			
1042 vw	991 vw			$\nu_s(CCC)$
1033 s	982 s	981 m		$\nu_s(CNC)$
	978 msh			
1032 m	974 m	973m		$\nu_s(CNC)$
	963 w	965 wsh		
	958 vwsh			
	952 w	952 vw		
	946 w	946 w		
	943 wsh	941 w		
	931 w	933 vwsh		
	924 w	926 vw		
	913 m	914 w		
	874 w	872 w		$\nu_s(CH_3)_2C$
	863 vw	860vwsh		
	857 vw			
993 w	849 vw			$\nu_s CCC$
990 wsh	830 wsh		832 vw	$\nu_s CNC$
	827 w	832 vwsh		
915 w	823 w	824 w		ωNH_2^+
	780 vw			
773 w	772 vw	767 wsh	762 vw	ωNH_2^+

	761 m			ρCH_2
	757 m	757 m		ρCH_2
		614vw		
	540 w			
	537 w	538 w		δCNC
		452 w		
	452 vw			
		426vw sh	426vw	
	420 vw	421vw		δCCN and δCCC
		378 vw		Lattice vibrations
		371vssh		
210 s			227 s	νSbBr(1) Ag
209 m		214 vs		νSbBr(1) Au
207 vs			222 s	νSbBr(3) Ag
206 s			209 vs	νSbBr(4) Ag
188 m		204vs		νSbBr(3) Au
187 m		201vssh		νSbBr(4) Au
			199 ssh	
			187msh	
179 m			107w	νSbBr(2) Ag
178 m		102 m	102 m	νSbBr(2^{ii}) Ag,Au
		84wsh	85 m sh	

vs – very strong; s – strong; m- medium; w – weak; vw– very weak; sh – shoulder; ν – stretching; δ – deformation, τ – twisting, ρ – rocking, ω – wagging; s – symmetric; a – asymmetric, t - torsion